RAMReS Sciences des Structures et de la Matière Vol. 6, N°1 (2022) 63 - 90
http://publication.lecames.org/index.php/mat ISSN: 2630-1180

# Study of the status of iron in clay materials from Côte d'Ivoire for their use as phosphate adsorbents

**Aké Aké Pierre[1,*], Coulibaly Vamoussa[1], Kouamé N'dri[1], Kedi Atolé Brice[2], Sei Joseph[1], Oyetola Samuel[1]**

[1]*Laboratoire de Constitution et Réaction de la Matière, UFR SSMT, Université Félix Houphouët Boigny, Abidjan, Côte d'Ivoire*
[2]*Laboratoire des sciences et technologies de l'environnement, UFR Environnement, Université Jean Lorougnon Guédé, Daloa, Côte d'Ivoire*

Received: 28 February 2022 / Received in revised form: 17 May 2022 / Accepted: 28 May 2022

***Abstract*:**

The mineralogical, textural and physicochemical characteristics of five clay samples from various regions of Côte d'Ivoire were studied by different methods. The characterization by X-ray diffraction revealed that a mineralogical composition of the samples are different. The minerals identified are chlorite, kaolinite, smectites, illite, quartz, goethite and rutile. Electron paramagnetic resonance and Mössbauer spectroscopy revealed the presence of structural iron, iron oxides and oxyhydroxides in the clay samples. The iron is mainly present at trivalent status in octahedral position. These samples are richer in fine particles. They develop relatively important specific surface area and have poor cristallinity.

***Keywords*:** Clay; Mineralogy; Goethite; Specific area; Resonance; Crystallinity.

*Corresponding author:
*Email address*: meake@yahoo.fr *(A.P. Aké)*

## 1. Introduction

Clays are the main components on the surface stratum of the earth's crust. They are constituted by silicates or aluminosilicates hydrated having a lamellar structure. They are essentially the result of the alteration of silicate rocks, such as feldspars. This natural raw material is constituted by clay minerals, which are associated with more or lowest abundant impurities such as quartz, feldspars, iron oxides and oxyhydroxides, calcite, organic matter, etc. Clays have been used by man since antiquity in many applications [1-5].

In addition to being abundant in the nature, clays are low cost. They are interesting materials due to their mineralogical and physicochemical properties: presence of electric charges on their surface, interesting fire behaviour (for the ceramist) [3], capacity of interfoliar cations exchange [3, 6]. Clays are extensively used in many industrial applications (pharmaceutical, medical, etc.) [7-13]. For example, clays are used as supports for filtering beverages (wines, beers, etc.) and eliminating metals, non-metals, anionic and cationic dyes in the production of drinking water. Some clays are used in poultices during difficult healing, for gastrointestinal dressings [7, 11, 14], beauty masks in cosmetics, elaboration of ceramic filters [15], concrete reinforcement [16], etc.

Since the development of these materials requires investigations, the objective of this work is to make mineralogical and physicochemical characterizations of some clay materials of Côte d'Ivoire in order to conclude on the possibility of using them in the depollution and the treatment of wastewater as adsorbents of metals and non-metals especially phosphorus. Indeed, phosphorus is introduced into aquatic environment from different point sources, mainly by domestic and industrial wastewater; contributing to the eutrophication of water bobies [17]. The consequences of eutrophication are multiple such as degradation of surface water quality. Eutrophication prevents aquatic sports, tourism and fishing activities. It constitutes a major environmental problem.

The most common way for wastewater dephosphation is the injection of expensive chemicals into the bodies of water [17]. In order to find an alternative to chemicals, adsorbents based on abundant natural materials, inexpensive and with high phosphorus adsorption capacities are increasingly used [18, 19]. Hence the interest in the clay materials of Côte d'Ivoire. It is worthy to notice that this country has many deposits according to geological studies conducted from 1963 to 1969 by the Mining Development Company (SODEMI) [20]. Beyond the environmental scope, the valorization of Côte d'Ivoire's clay materials is targeted.

## 2. Materials and experimental techniques

### 2.1. Clay samples

This study has been made with five clays from various regions of Côte d'Ivoire, a country in West Africa (Fig. 1). It is located at latitude 7°18'00,00" North and longitude 5°12'00,00" West. One sample from Anyama (District of Abidjan) noted ANY, one sample from Bondoukou noted BON, two samples from Katiola noted KAT 1 and KAT 2, and one sample from Korhogo noted KOR, have been used. The geographical coordinates of the sampling sites are shown in the table 1.

The clay samples were collected with a hoe. Then, the samples are put in nylon bags of 25 kg without preliminary treatment. Before characterization, the clay samples have been dried in the shade during several days, crushed and crumbled. A portion of each clay samples has been ground in an agate mortar. The resulting powder has been sieved to 100 µm.

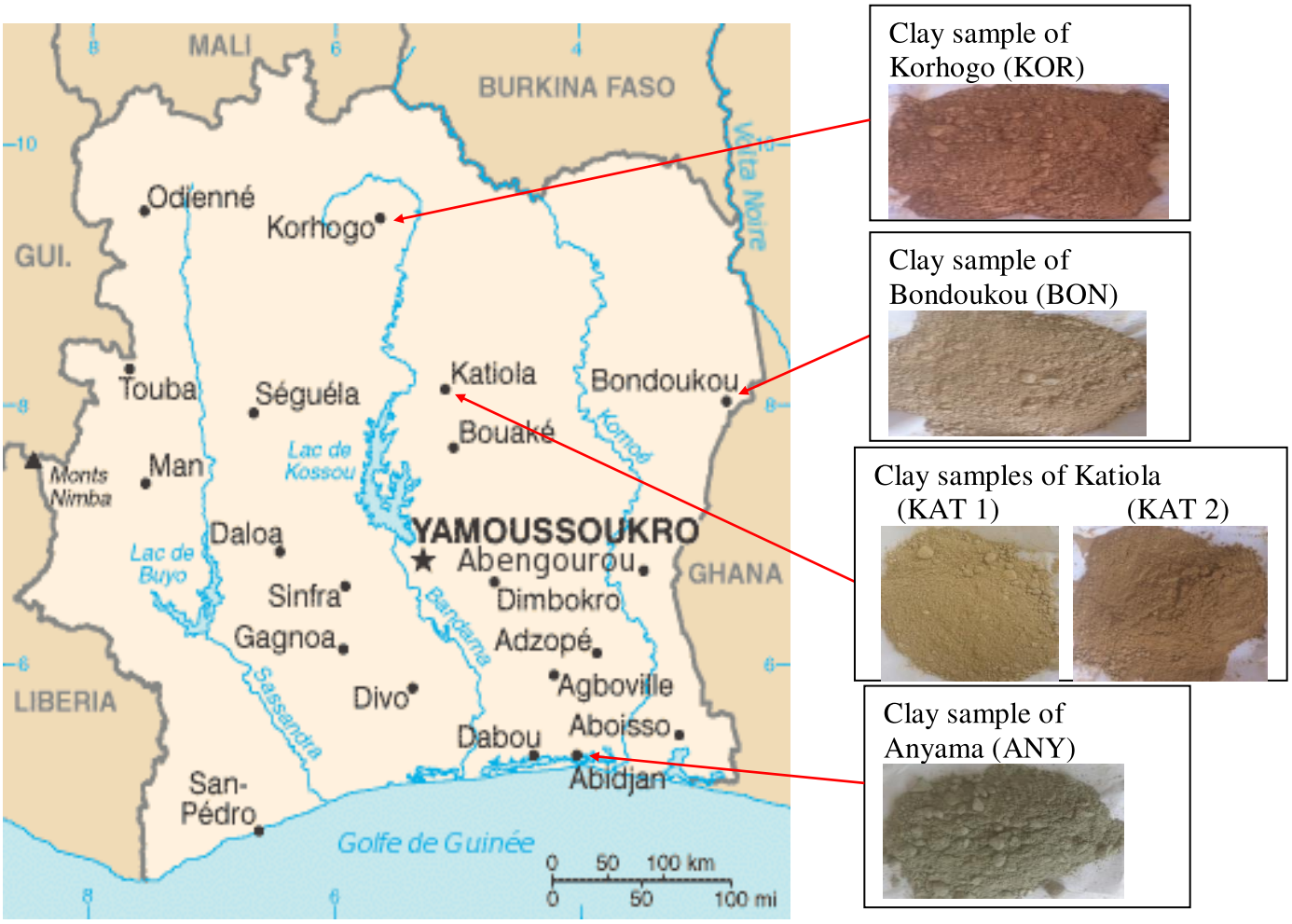


**Fig. 1.** Map of Côte d'Ivoire showing the regions where the clay samples have been taken.

**Table 1**
Geographical coordinates of the sampling sites.

| | Geographical coordinate | |
|---|---|---|
| **Sample** | **Latitude** | **Longitude** |
| ANY | 5°31'29" North | 4°03'14" West |
| BON | 8°02'23" North | 2°47'54" West |
| KAT 1 | 8°08'14" North | 5'37'46" West |
| KAT 2 | 8°08'22" North | 5'37'42" West |
| KOR | 9°27'28" North | 5°37'46" West |

### 2.2. Experimental analysis

The clay samples have been characterized by X-ray diffraction using a BRUKER D8 ADVANCE diffractometer. This diffractometer use the wavelength λ=1.7903 Å. The chemical analysis has been made using X-ray fluorescence with a SPECTRO X - LabPro spectrometer (XRF) coupled to a computer. For the X-ray fluorescence analysis, about 4 g of clay sample dried and ground have been mixed with 1 g of binding powder. The theoretical mineralogical composition of the clay samples has been calculated using Eq. (1) [21, 22] based on the chemical composition and the chemical formula of mineral phases:

$$T(a) = \sum_{i=1}^{n} M_i . P_i(a) \quad (1)$$

Where, T(a) is the content of element a in the material (%) ; $M_i$, is the content of mineral i in the material (%); $P_i(a)$, is the content of element a in the mineral i.

The morphology and the size of the minerals tablet in the sample structure, have been observed by a scanning electron microscope MEB using MEB FEG Supra 40 VP Zeiss equipment. This equipment contain an X-ray detector (OXFORD Instruments) connected to an EDS microanalyzer platform (Inca Dry Cool, without liquid nitrogen). For the analysis, about 5 mg of sample have been used.

The infrared spectra were obtained in the mid-infrared domain (wave numbers between 400 $cm^{-1}$ and 4000 $cm^{-1}$) using a Fourier Transformed Infra Red (FTIR) spectrometer.

The thermal analysis of the clay samples was studied from 303 K to 1473 K by differential scanning calorimetry (DSC) coupled with thermogravimetric (TG) analysis. These two analyses have been made simultaneously using a Platinum Evaluation V1.0.182 equipment.

The granulometric analysis has been made by sedimentation with the clay samples dried, crushed and sieved to 80 µm.

The cumulative efficiency of the particle sizes was used to set out a cumulative curve of particle sizes and to estimate the parameters $d_{90}$, $d_{75}$, $d_{50}$ and $d_{10}$. These parameters are the particle sizes (in µm) of the cumulative curve at y-axis 90%, 75%, 50% and 10%, respectively. The specific surface has been determined by BET method using nitrogen adsorption at 77 K.

Mössbauer spectra were recorded in transmission using a standard spectrometer. The source used is $^{57}Co$ in a rhodium matrix. The velocity has been calibrated at room temperature using six lines of α-iron spectra and all isomeric shifting have been given in relation to center of this spectra.

Electron paramagnetic resonance (EPR) spectra were recorded using a Bruker spectrometer operating at X-band (frequency υ=9.6 GHz) on crude samples. The parameters characteristic of EPR spectra (g), has been obtained in relation to standard value (DPPH, g = 2.0036) [23, 24].

The analysis has been made with crude clays, clays treated at 873 K and 1273 K.

## 3. Results and discussion

### 3.1. Chemical composition of clay samples

The chemical composition of the five clay samples is given in table 2. This table contains the main oxides.

The samples contain important quantity of silica (34.31 - 45.82%), appreciable quantity of alumina (14.59 - 25.19%) and iron oxide (3 - 8.22%). This observation shows that aluminosilicate phases and quartz are the main minerals in all of the samples. In addition, the samples contain very low quantities of phosphorus in $P_2O_5$ form (0.01 to 0.06%). The relatively low contents of titanium oxide $TiO_2$ (0.32 to 1.52%) and calcium oxide CaO (0.02 to 1.11%) indicate that the samples contains a little quantity of the titanium mineral (anatase, rutile, etc.) and calcium mineral (calcite, dolomite, etc.). The appreciable contents of iron oxide $Fe_2O_3$ (3 to 8.22%) may suggest that the samples contain a structural iron, iron oxides and iron hydroxides. The weight losses of the ANY and KAT 2 samples are 5.87 and 5.70%, respectively. These values are approximately equal to the theoretical weight loss of smectites which is 5% [25, 26]. It's shown a presence of smectites in ANY and KAT 2 samples. For the BON, KAT 1, and KOR samples, the weight losses vary from 10.13 to 11.44%. These weight losses are smaller than theoretical weight loss of kaolinite [25, 27-29]. However, these weight losses can indicate the presence of species hydrated in minerals structure.

**Table 2**
Chemical composition of the five clay samples in percent (%) of mass oxide.

| Sample | $SiO_2$ | $Al_2O_3$ | $Fe_2O_3$ | $K_2O$ | MgO | $TiO_2$ | $Na_2O$ | MnO | $P_2O_5$ | CaO | Weight loss |
|---|---|---|---|---|---|---|---|---|---|---|---|
| ANY | 44.90 | 16.77 | 7.59 | 2.53 | 3.06 | 0.94 | 0.30 | 0.06 | 0.03 | 0.02 | 5.86 |
| BON | 37.20 | 25.19 | 3.00 | 1.97 | 0.37 | 0.32 | 0.24 | 0.03 | 0.01 | 0.09 | 10.13 |
| KAT 1 | 45.82 | 18.21 | 8.20 | 1.06 | 2.08 | 0.90 | 0.78 | 0.02 | 0.03 | 1.11 | 10.42 |
| KAT 2 | 34.31 | 14.59 | 7.94 | 1.77 | 1.47 | 0.89 | 0.36 | 0.03 | 0.03 | 0.46 | 5.70 |
| KOR | 35.31 | 20.71 | 8.22 | 0.33 | 0.23 | 1.52 | 0.13 | 0.04 | 0.06 | 0.12 | 11.44 |

### 3.2. Mineralogical analysis

The X-ray diffraction spectra obtained are presented in figures 2-5. The diffractograms in figures 2 and 3 reveal that the ANY sample contains chlorite (lines at 14.09 Å; 7.06 Å; 4.71 Å; 3.53 Å and 2.82 Å), illite (lines at 9.94 Å ; 4.98 Å and 1.99 Å), and smectites (line at 14.83 Å (Fig. 3.a) and lines at 17.04 Å ; 8.49 Å and 5.75 Å (Fig. 3.b). These minerals are associated with quartz (lines at 4.25 Å; 3.34 Å; 2.28 Å; 2.13 Å and 1.82 Å), goethite (line at 2.57 Å) and rutile (lines at 3.2 Å and 2.46 Å). The diffractograms in figures 4 and 5 show that the BON, KAT 1, KAT 2, and KOR samples consist of kaolinite (lines at 7.15 - 7.17 Å ; 4.46 Å and 3.57 Å), illite (lines at 9.94 Å ; 4.98 Å and 1.99 Å), and quartz (lines at 4.25 Å ; 3.34 Å ; 2.28 Å ; 2.13 Å and 1.82 Å). In addition to these minerals, KAT 1 and KAT 2 samples also contain smectites (lines at 14.17 Å and 4.03 Å) and rutile (lines at 3.24 Å and 2.46 Å). BON sample contains goethite (lines at 4.15 Å and 2.56 Å), and KOR sample contains goethite (lines at 4.15 Å and 2.56 Å) and rutile (lines at 3.24 Å and 2.46 Å). Capital letters appearing in figures are defined below Fig. 5.

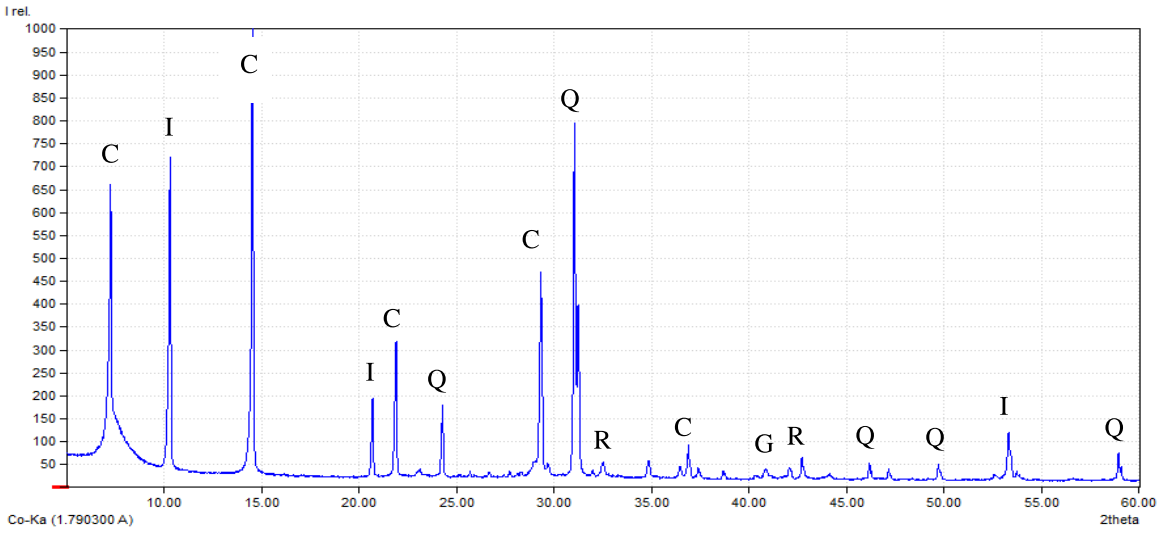


**Fig. 2.** X-ray diffractogram of the total rock of the ANY sample.

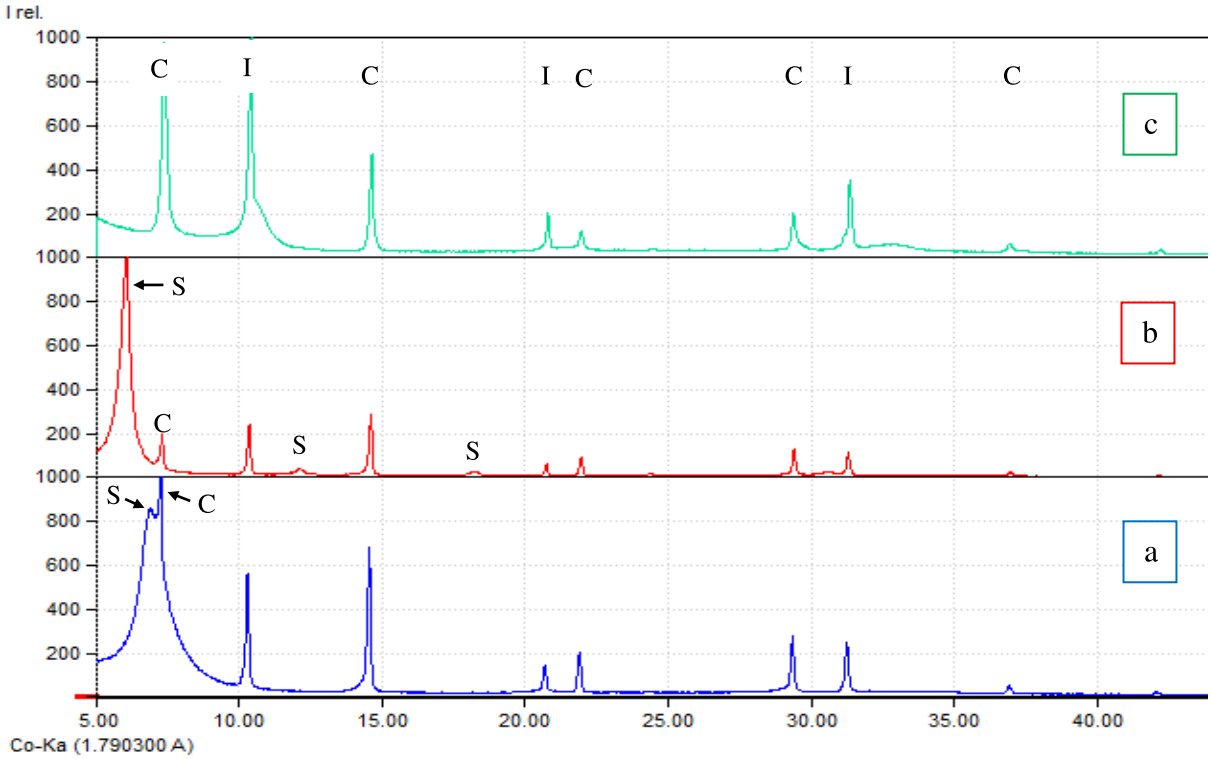


**Fig. 3.** X-ray diffractograms of the fine fraction of the ANY sample. (a) Normal slide; (b) Sample treated with ethylene glycol ; (c) Sample treated at 773 K.

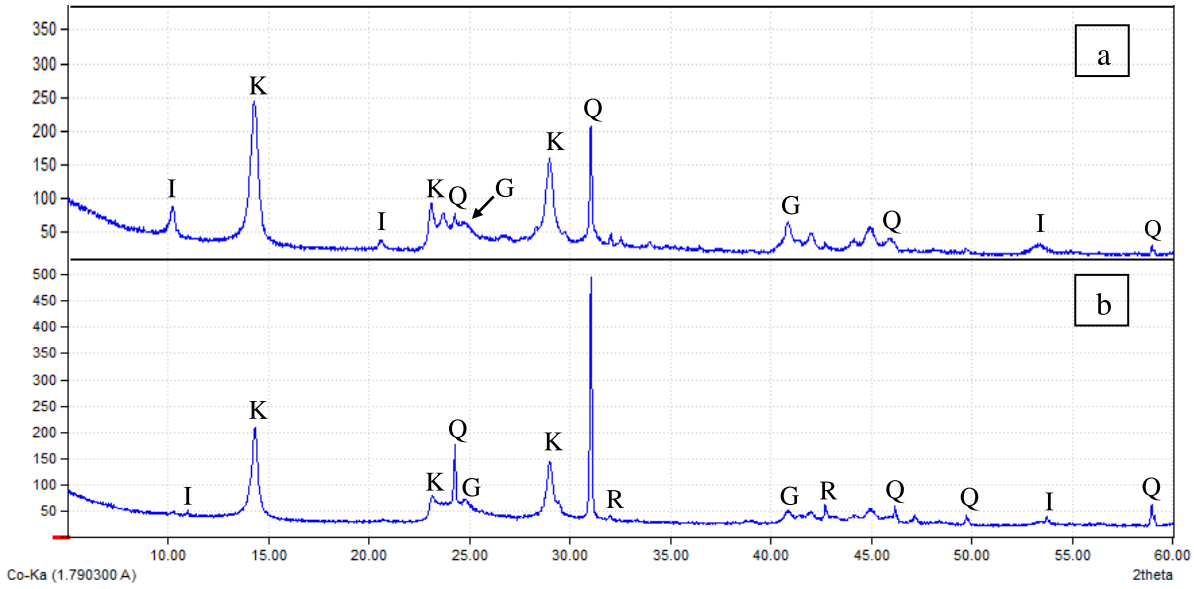


**Fig. 4.** X-ray diffractograms of the total rock of the (a) BON and (b) KOR samples.

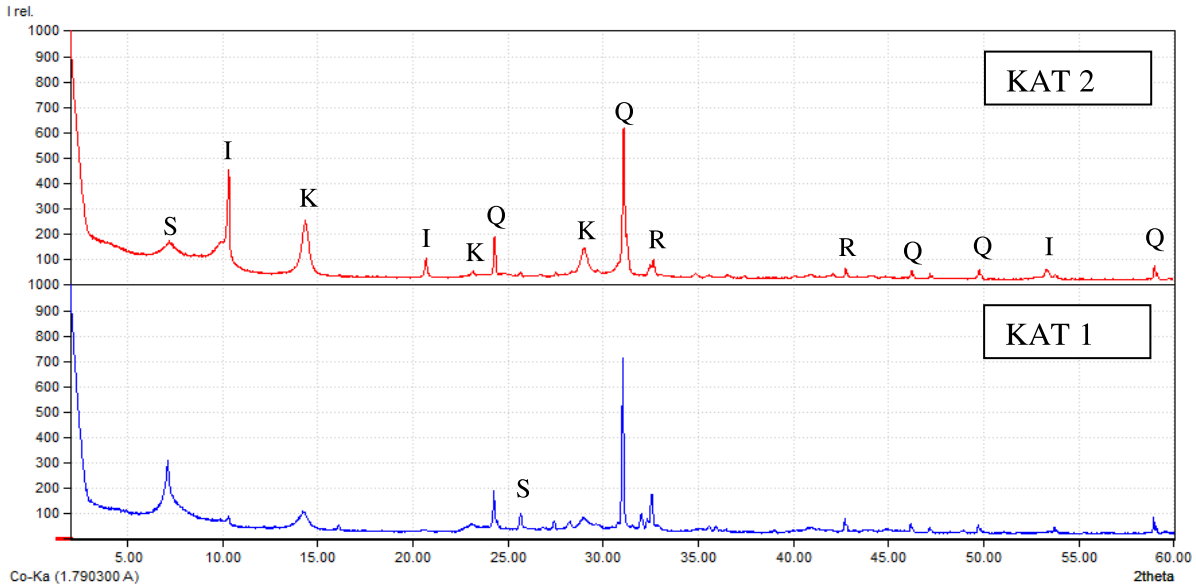


**Fig. 5.** X-ray diffractograms of the total rock of the KAT 1 and KAT 2 samples.
*C: chlorite; K: kaolinite; I: illite; S: smectite; G: goethite; R: rutile; Q: quartz.*

### 3.3. Mineralogical composition

The theoretical results of the mineralogical composition of the clay samples are shown in table 3.

The results show that ANY sample is richer in chlorite (23.54%), illite (21.44%) and quartz (25.69%) than the other four samples. However it contains the lowest content of smectites (12.50%). The highest smectites content (27.86%) is contained in KAT 1 sample. As for KOR sample, it is relatively rich in goethite (9.14%), kaolinite (49.71%) and rutile (1.52%). However it is less rich in illite (2.80%). Finally, BON sample has the lowest content of quartz (7.51%) and goethite (3.34%). The KAT 2 sample has the lowest content of kaolinite (22.35%). The presence of goethite in appreciable quantity, could make the ANY and KOR samples particularly adsorbent.

**Table 3**
Proportion of the mineral phases of the clay samples.

| Sample | % Chlorite | % Goethite | % Illite | % Kaolinite | % Quartz | % Smectite | % Rutile | Total |
|---|---|---|---|---|---|---|---|---|
| ANY | 23.54 | 8.44 | 21.44 | - | 25.69 | 12.5 | 1 | 92.61 |
| BON | - | 3.34 | 16.69 | 47.55 | 7.51 | - | - | 75.09 |
| KAT 1 | - | - | 8.98 | 37.37 | 24.38 | 27.86 | 1 | 99.59 |
| KAT 2 | - | - | 15.00 | 22.35 | 17.14 | 20.90 | 1 | 76.39 |
| KOR | - | 9.14 | 2.80 | 49.71 | 10.93 | - | 1.52 | 74.10 |

### 3.4. Morphology of the clayey platelets

The figure 6 shows the morphology of the five samples (ANY, BON, KAT 1, KAT 2 and KOR).

The morphology of the ANY sample in figure 6.a, shows a lamellar structure parallel; such an arrangement can indicate the presence of pores. Concerning BON sample (Fig. 6.b), the particles appearing as hexagonal tablets with regular surface, suppose a well kaolinite crystallized [30]. These hexagonal tablets are stacked on top of each other (face-to-face crystals) and, they form crystal piles of 2 µm thick approximately. In KAT 1 and KAT 2 samples, the morphology (Fig. 6.c and Fig. 6.d) shows a lamellar structure superposed with edges rolled and undulations. The morphology of the KOR sample (Fig. 6.e) shows a lamellar structure that is difficult to observe; the structures are disrupted. This sample has the appearance of porous material.

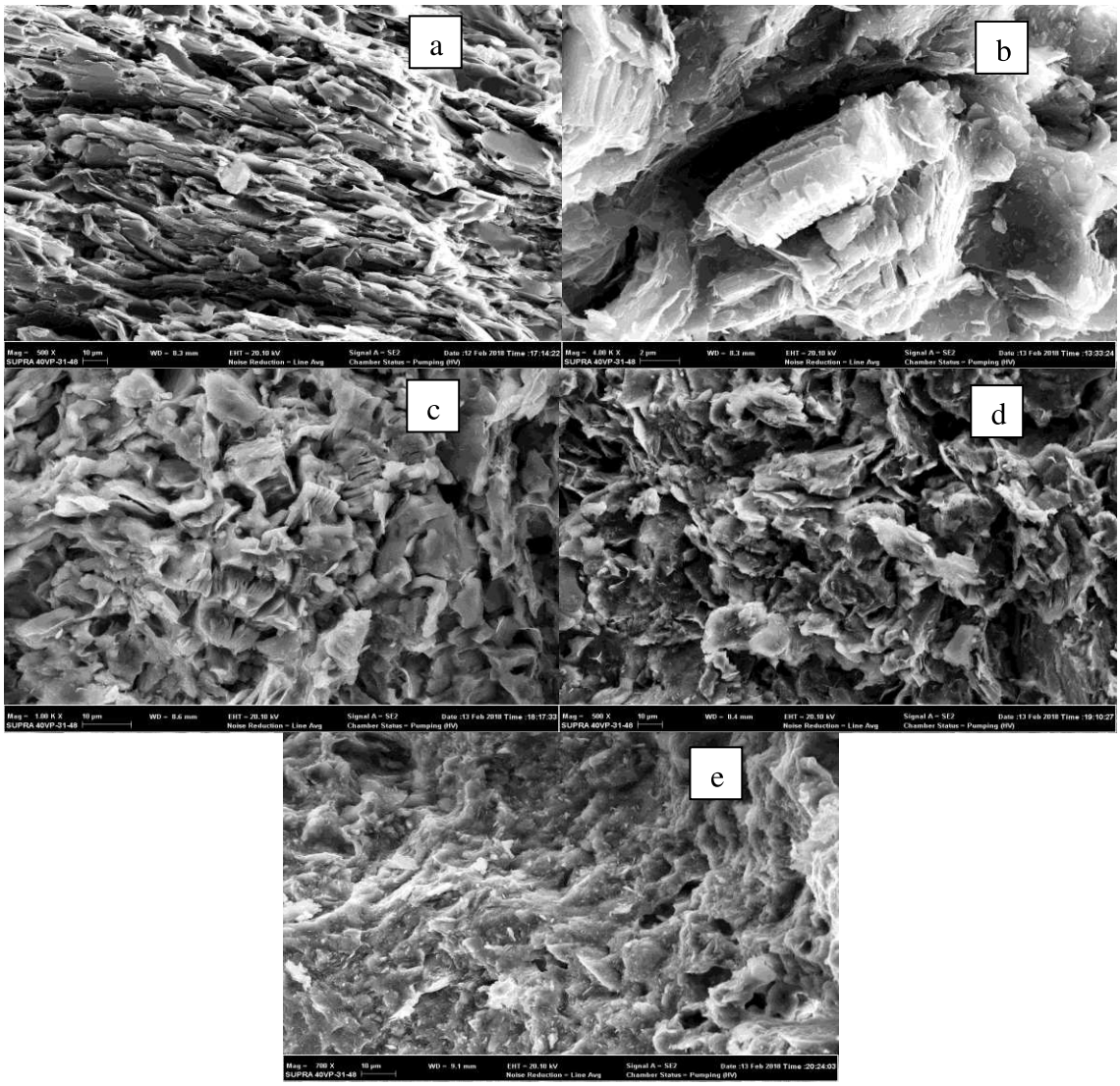


**Fig. 6.** Morphology of the clay samples: (a) ANY; (b) BON; (c) KAT 1; (d) KAT 2; (e) KOR.

### 3.5. Infrared spectroscopy

The infrared spectra of the ANY, BON, KAT 1, KAT 2 and KOR samples are presented in figure 7. The wave numbers observed are given in table 4. The infrared spectra of the BON sample (Fig. 7.b) and KOR sample (Fig. 7.e), present a similar pace. The KAT 1 sample (Fig. 7.c) and the KAT 2 sample (Fig. 7.d), present also a similar pace. In the domain 3500 - 4000 $cm^{-1}$, the BON and KAT 1 samples show two bands attributed to elongation vibration of $Al_2OH$ group in the kaolinite structure. The KAT 2 and KOR samples show three bands. The band appearing at 3620 $cm^{-1}$ is observed in all samples. It characterizes the elongation vibration of middle plane hydroxyls OH group (also called internal hydroxyls). These hydroxyls OH consisted of both mineral 1:1 structure (kaolinite, dickite, nacrite) and mineral 2:1 structure (illite) [2]. The bands at 3649 and 3689-3693 $cm^{-1}$ characterize the elongation vibration of the hydroxyls OH present in the interfoliar space (also called external hydroxyls). The band at 3649 $cm^{-1}$, present only in KAT 2 and KOR samples, are resulted from the coupling of two external hydroxyls OH in phase opposition [5]. The band at 3689 $cm^{-1}$ in BON sample, 3693 $cm^{-1}$ in KAT 1 sample and 3692 $cm^{-1}$ in KAT 2 and KOR samples are attributed to an external hydroxyls OH forming an angle of 76° with the crystallographic c-axis [5]. The low intensity of the bands close to 3700 $cm^{-1}$, can indicate a poor crystallinity of clays material [31].

In addition, the wide band at 3397 $cm^{-1}$ observed in the spectra of ANY sample (Fig. 7.a) and KAT 1 sample (Fig. 7.c), has been attributed to the elongation vibration of hydroxyls OH in water adsorbed structure [2]. In the domain 700 - 1800 $cm^{-1}$, the vibrations of the Si-O groups and the vibration of deformation of hydroxyls OH in phyllosilicates appear [5, 32]. In the spectra of figures 7.b - 7.e, the bands of average intensity at 684, 749-757 and 785-789 $cm^{-1}$ correspond to vibration of hydroxyls OH that are perpendicular to the surface (also called translational hydroxyls OH) [33, 34]. The last two bands were used to estimate the crystallinity and the degree of order in kaolinite structure [35]. When the kaolinite is well-crystallized, these two bands have the same intensity. But in kaolinite disordered, the intensity of these two bands is different. The intensity of these two bands is not strong in the samples BON, KAT 1, KAT 2 and KOR; this suggests that these samples are moderately ordered. In all samples, the vibration of deformation of $Al_2OH$ groups (for internal hydroxyl) is observed at 909 - 912 $cm^{-1}$. In addition, the bands at 1654 $cm^{-1}$ in ANY sample, 1634 $cm^{-1}$ in KAT 1 sample and 1637 $cm^{-1}$ in KAT 2 sample, have been attributed to the vibration of deformation of hydroxyls OH in the water adsorbed structure [36 - 39]. In the ANY sample, the bands at 1452, 2125 and 2243 $cm^{-1}$ with low intensity correspond to the elongation vibration of CO groups in calcite structure [7]. For this sample, calcite could not be detected by XRD, probably because of the little quantity.

The strong bands at 999, 1000, 1001, 1024 and 1113 $cm^{-1}$ are assigned to elongation vibration of Si-O bonds [32, 38].

In ANY sample, the band appearing at 685 $cm^{-1}$, has been attributed to the vibration of deformation of hydroxyls OH in mica structure and in lamellar structure [2]. The samples studied shows bands at 451-461 $cm^{-1}$ and 512-530 $cm^{-1}$. They are assigned to the vibration of deformation of Si-O bonds [16, 40] and deformation of Si-O-Al [16, 38], respectively. Al is located in tetrahedral site in samples KAT 1 and KAT 2, and in octahedral site in samples ANY, BON and KOR.

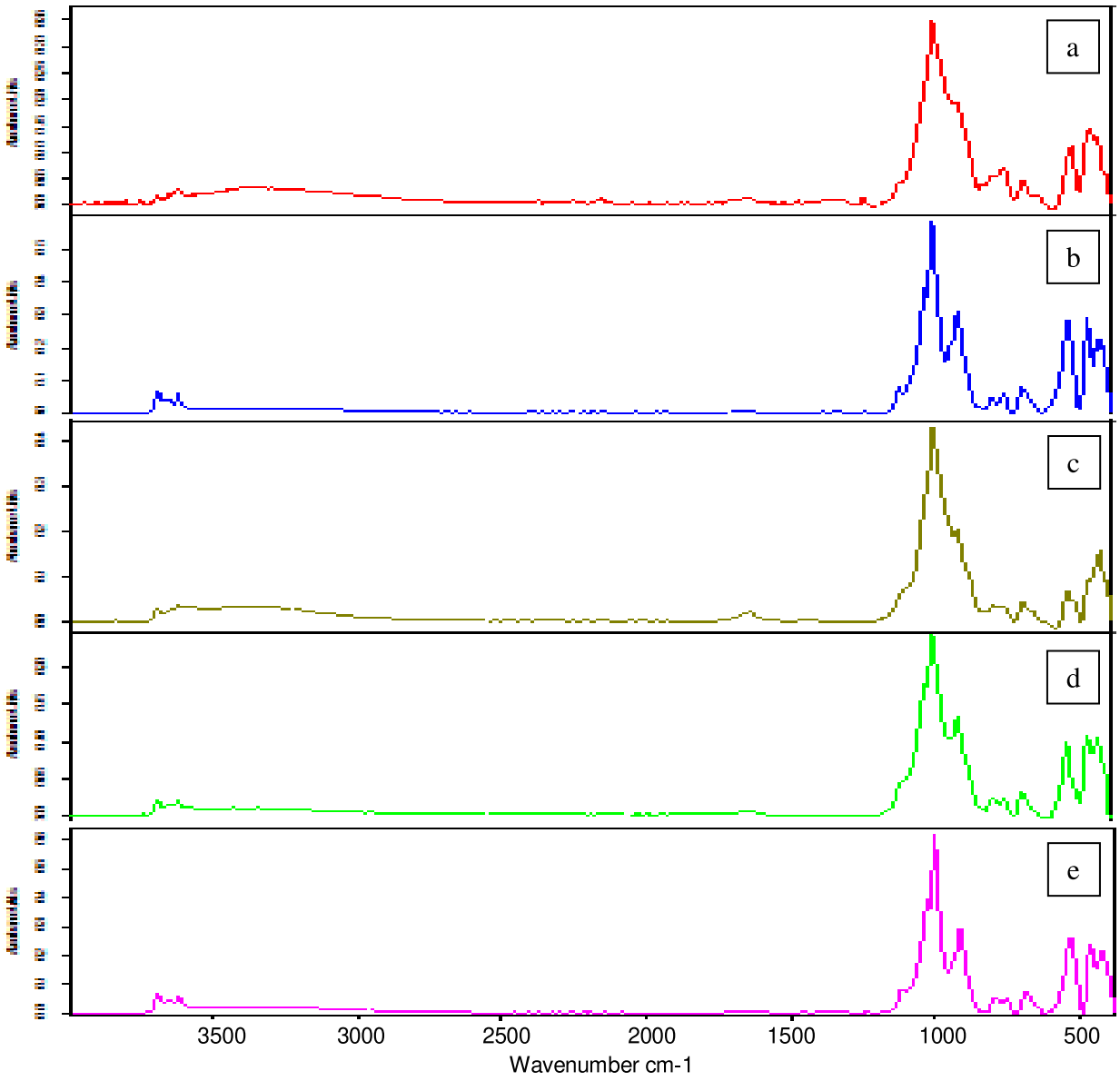


**Fig. 7.** IR spectra of the (a) ANY; (b) BON; (c) KAT 1; (d) KAT 2 and (e) KOR samples.

**Table 4**
Wave numbers observed in the clay samples.

| Sample | Wave number | Attribution |
|---|---|---|
| ANY | 3619 $cm^{-1}$ | Elongation vibration of internal OH |
| | 3396 $cm^{-1}$ | Elongation vibration of OH in water adsorbed structure |
| | 2243 $cm^{-1}$ | Elongation vibration of CO group in calcite structure |
| | 2145 $cm^{-1}$ | Elongation vibration of CO group in calcite structure |
| | 1654 $cm^{-1}$ | Vibration of deformation of OH in water adsorbed structure |
| | 1452 $cm^{-1}$ | Elongation vibration of CO group in calcite structure |
| | 1000 $cm^{-1}$ | Elongation vibration of Si-O |
| | 912 $cm^{-1}$ | Vibration of deformation of $Al_2OH$ (internal OH) |
| | 751 $cm^{-1}$ | Elongation vibration of Si-O |
| | 685 $cm^{-1}$ | Vibration of deformation of OH in mica structure |
| | 512 $cm^{-1}$ | Vibration of deformation of Si-O-Al (octahedral Al) |
| | 451 $cm^{-1}$ | Vibration of deformation of Si-O bonds |
| BON | 3689 $cm^{-1}$ | Elongation vibration of external OH |
| | 3620 $cm^{-1}$ | Elongation vibration of internal OH |
| | 1113 $cm^{-1}$ | Elongation vibration of Si-O |
| | 1024 $cm^{-1}$ | Elongation vibration of Si-O |
| | 912 $cm^{-1}$ | Vibration of deformation of $Al_2OH$ (internal OH) |
| | 788 $cm^{-1}$ | Vibration of OH perpendicular to the surface (kaolinite) |
| | 751 $cm^{-1}$ | Vibration of OH perpendicular to the surface (kaolinite) |
| | 684 $cm^{-1}$ | Vibration of OH perpendicular to the surface (kaolinite) |
| | 528 $cm^{-1}$ | Vibration of deformation of Si-O-Al (octahedral Al) |
| | 460 $cm^{-1}$ | Vibration of deformation of Si-O bonds |
| KAT 1 | 3693 $cm^{-1}$ | Elongation vibration of external OH |
| | 3620 $cm^{-1}$ | Elongation vibration of internal OH |
| | 3397 $cm^{-1}$ | Elongation vibration of OH in water adsorbed structure |
| | 1634 $cm^{-1}$ | Vibration of deformation of OH in water adsorbed structure |
| | 999 $cm^{-1}$ | Elongation vibration of Si-O |
| | 910 $cm^{-1}$ | Vibration of deformation of $Al_2OH$ (internal OH) |
| | 785 $cm^{-1}$ | Vibration of OH perpendicular to the surface (kaolinite) |
| | 757 $cm^{-1}$ | Vibration of OH perpendicular to the surface (kaolinite) |
| | 684 $cm^{-1}$ | Vibration of OH perpendicular to the surface (kaolinite) |
| | 529 $cm^{-1}$ | Vibration of deformation of Si-O-Al (tetrahedral Al) |
| | 421 $cm^{-1}$ | Vibration of deformation of Si-O bonds |

**Table 4** (*continued*)

| Sample | Wave number | Attribution |
|---|---|---|
| KAT 2 | 3692 $cm^{-1}$ | Elongation vibration of external OH |
| | 3650 $cm^{-1}$ | Elongation vibration of external OH |
| | 3619 $cm^{-1}$ | Elongation vibration of internal OH |
| | 1637 $cm^{-1}$ | Vibration of deformation of OH in water adsorbed structure |
| | 1024 $cm^{-1}$ | Elongation vibration of Si-O |
| | 999 $cm^{-1}$ | Elongation vibration of Si-O |
| | 910 $cm^{-1}$ | Vibration of deformation of $Al_2OH$ (internal OH) |
| | 790 $cm^{-1}$ | Vibration of OH perpendicular to the surface (kaolinite) |
| | 750 $cm^{-1}$ | Vibration of OH perpendicular to the surface (kaolinite) |
| | 685 $cm^{-1}$ | Vibration of OH perpendicular to the surface (kaolinite) |
| | 530 $cm^{-1}$ | Vibration of deformation of Si-O-Al (tetrahedral Al) |
| | 461 $cm^{-1}$ | Vibration of deformation of Si-O bonds |
| | 425 $cm^{-1}$ | Vibration of deformation of Si-O bonds |
| KOR | 3692 $cm^{-1}$ | Elongation vibration of external OH |
| | 3649 $cm^{-1}$ | Elongation vibration of external OH |
| | 3620 $cm^{-1}$ | Elongation vibration of internal OH |
| | 1113 $cm^{-1}$ | Elongation vibration of Si-O |
| | 1024 $cm^{-1}$ | Elongation vibration of Si-O |
| | 1001 $cm^{-1}$ | Elongation vibration of Si-O |
| | 910 $cm^{-1}$ | Vibration of deformation of $Al_2OH$ (external OH) |
| | 790 $cm^{-1}$ | Vibration of OH perpendicular to the surface (kaolinite) |
| | 749 $cm^{-1}$ | Vibration of OH perpendicular to the surface (kaolinite) |
| | 684 $cm^{-1}$ | Vibration of OH perpendicular to the surface (kaolinite) |
| | 528 $cm^{-1}$ | Vibration of deformation of Si-O-Al (octahedral Al) |
| | 460 $cm^{-1}$ | Vibration of deformation of Si-O bonds |

### 3.6. Thermal analysis

The DSC curve of the ANY sample (Fig. 8), shows five endothermic effects.

The first peak at 57 °C, producing a mass loss about 1.77%, is attributed to the elimination of hygroscopic waters. At about 213 °C, the second endothermic phenomenon is accompanied by a relatively little mass loss (0.21%). It is due to the elimination of water from interfoliar cations. The other endothermic effects are observed at 504 °C, 615 °C and 759 °C. They are assigned to the elimination of strutural hydroxyls (dehydroxylation) from the octahedral position, dehydration of brucitic layers and the decomposition of mica layers in chlorite structure, respectively [2]. All these phenomena cause the loss of constitution waters and they produce mass loss about 3.49%.

The figure 9 shows the DSC curves of the BON and KOR samples.

Between 50 °C and 200 °C, the DSC curves of the BON sample (Fig. 9.a) and the KOR sample (Fig. 9.b) show endothermic effects accompanied by mass loss about 0.84% for BON sample and 0.96% for KOR sample. They are attributed to the elimination of hydroscopic waters. In the domain 450 °C and 550 °C, each sample shows a strong endothermic effect. This phenomenon is attributed to the elimination of the structural hydroxyls (dehydroxylation) of octahedral position in kaolinite structure and it leads to the formation of metakaolinite [20, 41]. This dehydroxylation reaction given by Eq. (2) [20, 21, 39], shows a mass loss about 8.7% for BON sample and 8.03% for KOR sample.

$$\underset{\textit{kaolinite}}{Si_2Al_2O_5(OH)_4} \longrightarrow \underset{\textit{metakaolinite}}{Si_2Al_2O_7} + 2\,H_2O \qquad (2)$$

The exothermic effects appearing at 955 °C in KOR sample and 980 °C in BON sample correspond to the structural reorganization of metakaolinite leading to a spinel phase and an amorphous silica according to Eq. (3) [20, 42].

$$\underset{\textit{metakaolinite}}{2\,Si_2Al_2O_7} \longrightarrow \underset{\textit{spinel}}{Si_3Al_4O_{12}} + SiO_2 \qquad (3)$$

Between 200 °C and 400 °C, the DSC curve of the KOR sample (Fig. 8.b) shows two endothermic effects (peaks at 220 °C and 343 °C) and one exothermic effect (peak at 302 °C). The mass loss associated with these effects is about 0.99%. The peak at 220 °C would be due to the transformation of goethite FeOOH into haematite α-$Fe_2O_3$ according to the following reaction [43]:

$$2\,FeOOH \longrightarrow Fe_2O_3 + H_2O \qquad (4)$$

This deshydroxylation occurs between 200 °C and 350 °C [43].

The peak at 302 °C could be attributed to the decomposition of organic matter [43]. The peak at 343 °C would probably be due to the decomposition of associated amorphous substances, for example, with iron-silica or aluminium-silica gels [20].

The DSC curves of the KAT 1 sample (Fig. 10.a) and the KAT 2 sample (Fig. 10.b) show five endothermic effects and one exothermic effect. Between 50 °C and 100 °C, two endothermic phenomena are observed. They correspond to the elimination of hydroscopic waters. The mass loss produced is about 5.19% in KAT 1 sample and 1.61% in KAT 2 sample.

In the domain 100 °C and 210 °C, the DSC curve of sample KAT 1 shows two endothermic phenomena, one at 170 °C and the other at 206 °C. They could be assigned to the elimination of water from interfoliar cations. This transformation appears also at 148 °C, in the KAT 2 sample (Fig. 10.b). Then, the medium endothermic effects at 491 °C for KAT 1 sample and 495 °C for KAT 2 sample, associated to mass loss (3.74% for KAT 1 sample and 3.66% for KAT 2 sample), have been attributed to the elimination of the structural hydroxyls (dehydroxylation) of octahedral position in kaolinite structure. The end of the DSC curves show at 909 °C (for KAT 1) and 953 °C (for KAT 2), an exothermic phenomenon without mass loss. It could correspond to the structural rearrangement of metakaolinite. In addition, the DSC curve of the KAT 2 sample (Fig. 10.b) shows a thermal accident at 573 °C. It's attributed to the allotropic transformation of quartz α into quartz β [2, 15].

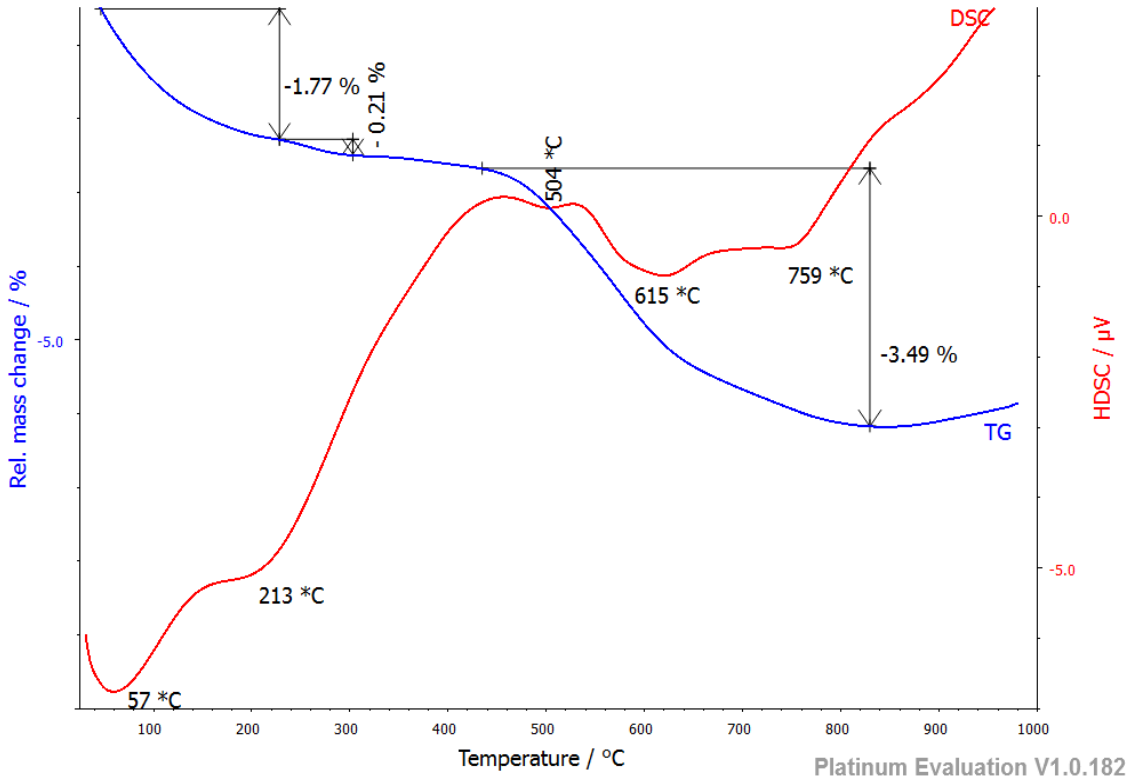


**Fig. 8.** DSC and TGA curves of the ANY sample.

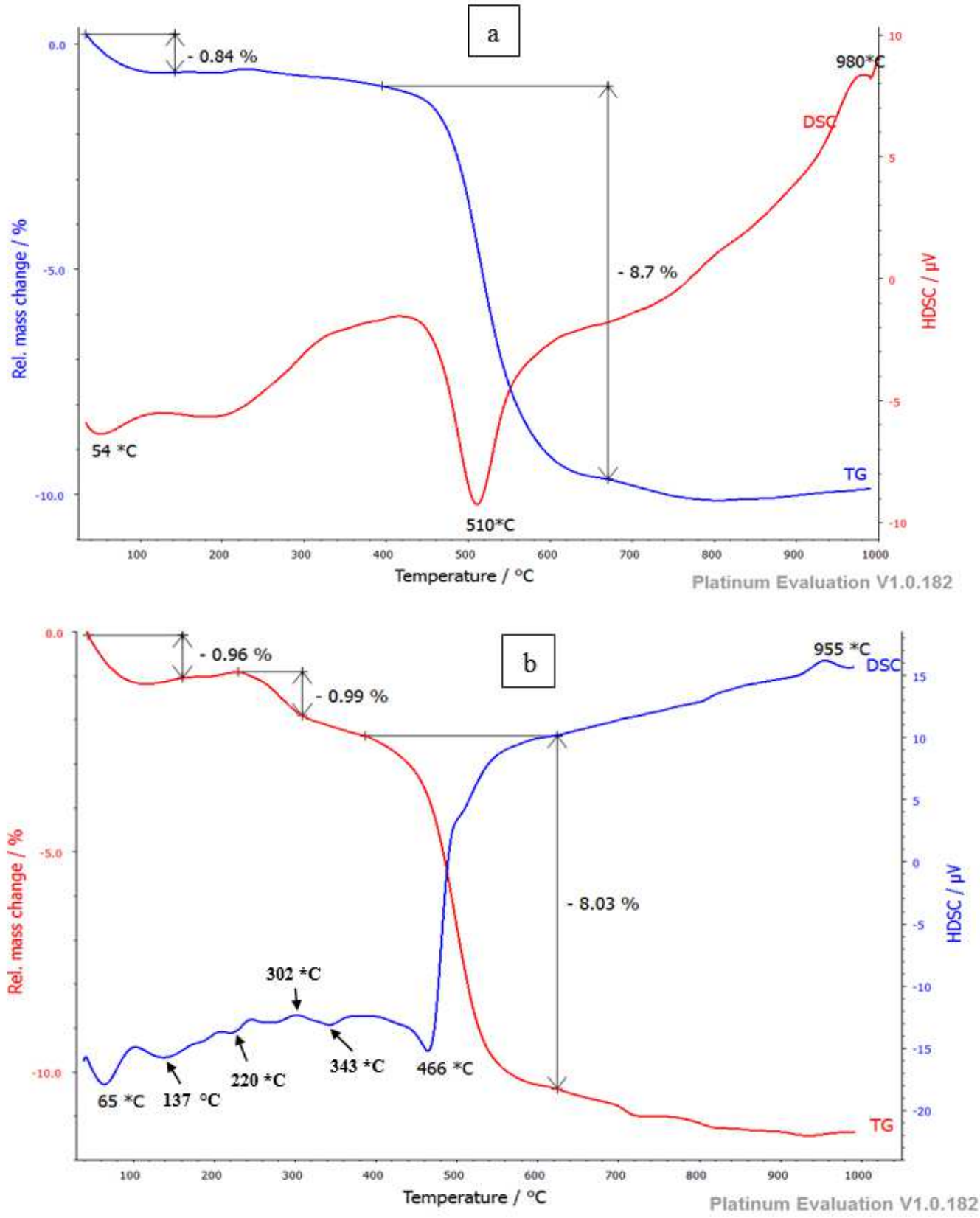


**Fig. 9.** DSC and TGA curves of the (a) BON and (b) KOR samples.

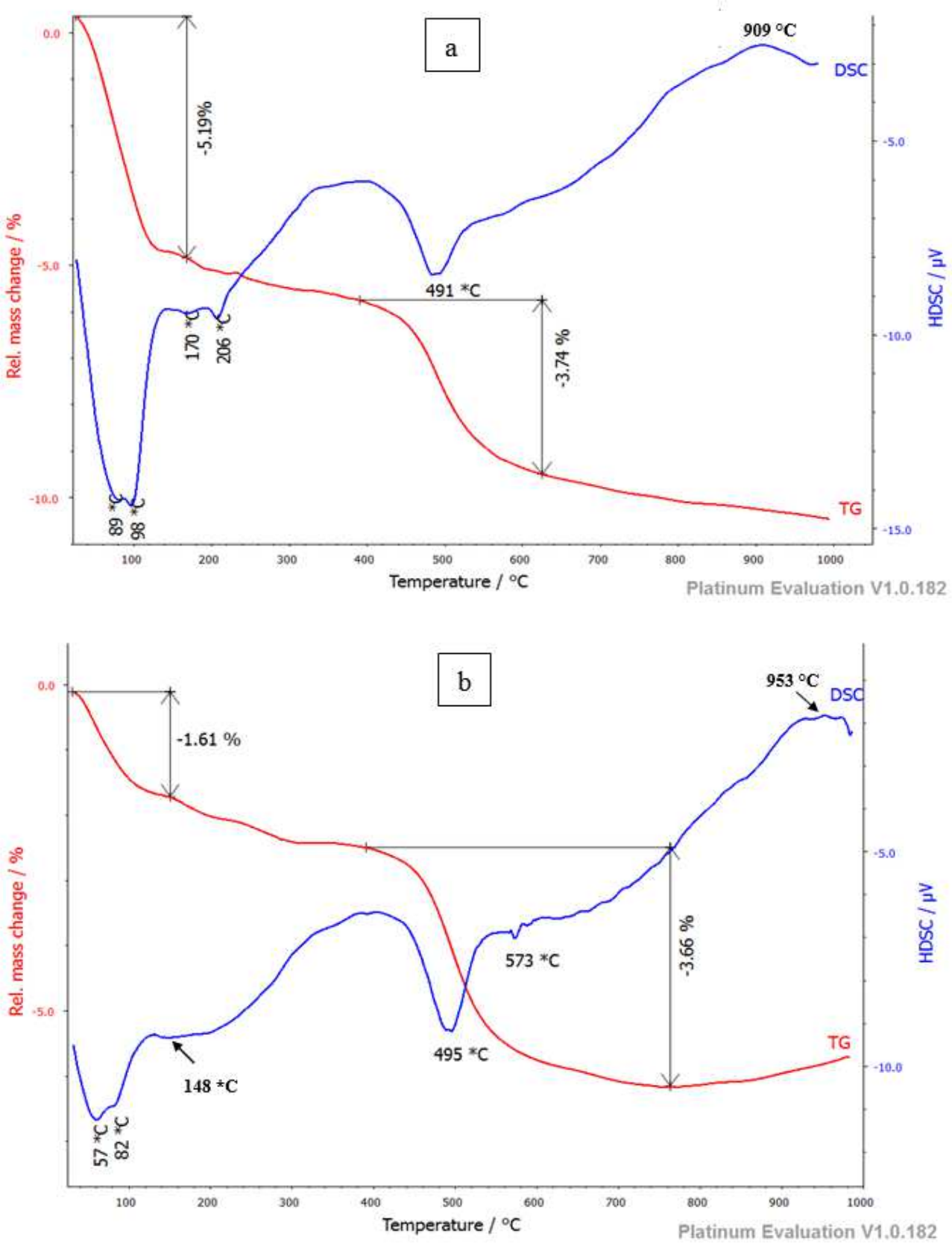


**Fig. 10.** DSC and TGA curves of the (a) KAT 1 and (b) KAT 2 samples.

### 3.7. Granulometric analysis

The parameters $d_{90}$, $d_{75}$, $d_{50}$ and $d_{10}$ deduced from cumulative curve of particle sizes (Fig. 11) are reported in table 5.

The analysis of the particle sizes distribution reveals that:

- the most of particle sizes varie between 1 µm and 70 µm. This fraction represents about 98% of clay samples sieved. This indicates that the clay samples studied, are characterized by a great fineness of the particles;
- 10% of particles of the ANY, BON, KAT 1, KAT 2 and KOR samples have diameters smaller than 1.59 µm, 1.51 µm, 1.57 µm, 1.53 µm and 1.39 µm, respectively ;
- 50% of particles of the ANY, BON, KAT 1, KAT 2 and KOR samples have diameters smaller than or equal to 8.25 µm, 3.3 µm, 9.35 µm, 10.5 µm and 1.39 µm, respectively ;
- 75% of particles of the ANY, BON, KAT 1, KAT 2 and KOR samples have diameters smaller than or equal to 15.8 µm, 9.5 µm, 26.75 µm, 24.5 µm and 6 µm, respectively ;
- 90% of particles of the ANY, BON, KAT 1, KAT 2 and KOR samples have diameters smaller than 29.25 µm, 18.25 µm, 43.25 µm, 41 µm and 20.3 µm, respectively.

The KOR sample is richer in fine particles than the other samples because it has a lowest parameter of $d_{50}$. The BON sample is the second sample rich in fine particles. The particles of KAT 2 sample have big diameters. The fineness of particles could be resulted to the poor crystallinity of clay materials [20]; this can probably give important specific surface. The ANY, KAT 1 and KAT 2 samples have relatively bigger parameter of $d_{50}$. According to Konan [4], a strong agglomeration of the particles resulting from poor dispersion of the suspension could explain these results.

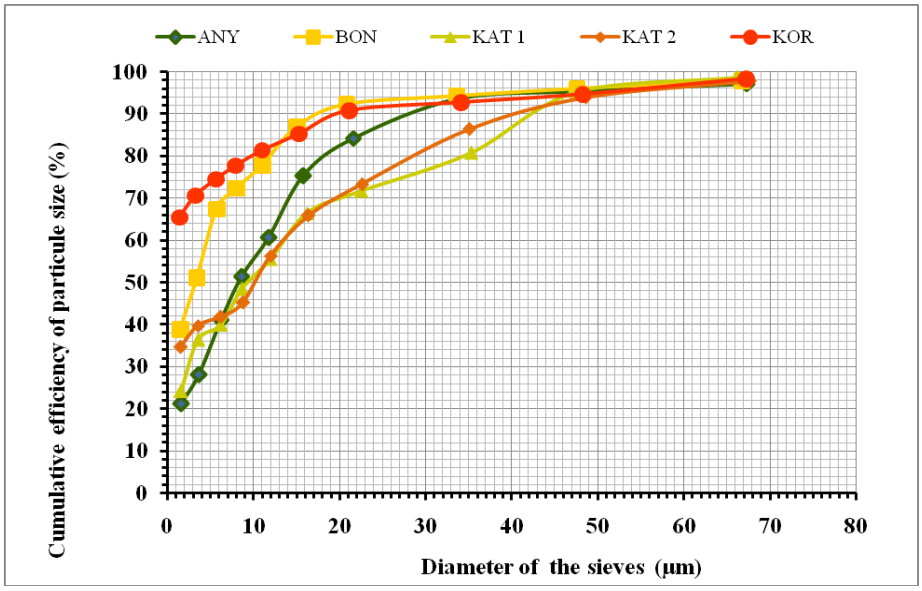


**Fig. 11.** Cumulative curve of particle sizes.

**Table 5**
Particle sizes of the clay samples studied.

| | Particle size (µm) | | | |
|---|---|---|---|---|
| Sample | $d_{90}$ | $d_{75}$ | $d_{50}$ | $d_{10}$ |
| ANY | 29.25 | 15.80 | 8.25 | < 1.59 |
| BON | 18.25 | 9.50 | 3.30 | < 1.51 |
| KAT1 | 43.25 | 26.75 | 9.35 | < 1.57 |
| KAT2 | 41 | 24.50 | 10.50 | < 1.53 |
| KOR | 20.3 | 6 | < 1.39 | < 1.39 |

### 3.8. Specific surface area

The specific surface area and density of the clay samples studied are given in table 6.

The results show that the clay sample have similar specific surface area and density. The specific surface area is between 40.17 and 41.86 $m^2 g^{-1}$, and the density is between 2.42 and 2.57 g $cm^{-3}$. The BON and KOR samples have an important specific surface area when they are consisted mostly of kaolinite (clay mineral 1:1) because the BON sample contains 47.55 % of kaolinite and the KOR sample 49.71 %. These important specific surfaces area result from the quantity of iron oxides. Indeed, the presence of iron oxides in materials, contributes strongly to the increase of the specific surface area [44, 45]. According to the data of table 5, the BON and KOR samples are consisted of particles for which the mean diameters (≈ 3.3 µm for BON and < 1.39 µm for KOR) are smaller than the mean diameter particles of samples ANY (≈ 8.25 µm), KAT 1 (≈ 9.35 µm) and KAT 2 (≈ 10.5 µm). Thus, in addition to the presence of goethite, the particles size of clays material is another parameter to consider in the explanation of important specific surface. This observation has been made by Konan [4].

**Table 6**
Specific surface area and density of the clay samples studied.

| Sample | ANY | BON | KAT 1 | KAT 2 | KOR |
|---|---|---|---|---|---|
| Specific surface area ($m^2 g^{-1}$) | 40.17 | 41.35 | 41.86 | 40.61 | 40.45 |
| Apparent density (g $cm^{-3}$) | 2.57 | 2.47 | 2.42 | 2.54 | 2.56 |

### 3.9. Electron paramagnetic resonance (EPR)

The resonances observed in the ANY, BON and KAT 1 samples are given in table 7. The EPR spectra are presented in figures 12-14.

In strong fields (between 2500 and 4000 G), the spectrum of the raw ANY sample (Fig. 12.a) shows a wide resonance and an asymmetric signal at 3510 G (g=2.05). The asymmetric signal with a medium intensity, is consisted of two fine lines. This signal has been attributed in the literature to the crystal imperfections (holes) [25, 46]; this seems to indicate that the ANY sample contains holes (defects localized).

The wide resonance present in the strong field is also observed in BON and KAT 1 samples between 2000 and 4000 G. It's attributed to the iron richer phases that are iron oxides (haematite), iron oxyhydroxides (goethite) and iron gels [5, 25]. This result could justify the relative important quantity of $Fe_2O_3$ in the clay samples studied (Table 2) and the presence of goethite detected by XRD in the ANY and BON samples.

In the weak fields (between 400 and 2000 G), the ANY sample shows a signal consisted of four lines well-marked (Fig. 13.a). On the other hand, the spectrum of the raw KAT 1 sample shows a very weak signal (Fig. 14.a). This signal is attributed to $Fe^{3+}$ ions in octahedral environment position (spin S=5/2). The $Fe^{3+}$ ions occupy two different distortion sites, denoted as Fe (A) and Fe (B) [5, 25]. The $Fe^{3+}$ ions from site A are reported at 1590 G (g=4.53) and 1690 G (g=4.23) in BON and KAT 1 samples, respectively. These iron ions belong to the octahedral environment with rhombic distortion located at the limits of the coherent X-ray diffraction domains; this confirms the presence of kaolinite in the BON and KAT 1 samples. Indeed, according to Delineau et al. [47], these types of iron ions are always observed in kaolinites. The $Fe^{3+}$ ions of site B present in the BON sample, give on the spectrum of figure 12.a, a signal consisted of three lines. They belong to octahedral environments with less rhombic distortion, i.e. regions of high crystallinity and regular stacking. This result could justify the arrangement of the clay tablets in this sample (Fig. 6.b).

When the temperature of the treatment increases:

- the wide resonance attributed to the iron rich phases shrinks in the samples. But in sample BON, the intensity of this resonance decreases to reach its minimum at 873 K, then the intensity of this resonance increases during treatment to 1273 K. This result suggests that the BON sample does not contain iron oxides of the same nature as those of the ANY and KAT 1 samples;
- the fine lines at g=2.05 and the line at 1590 G (g=4.53) attributed to octahedral $Fe^{3+}$ ions of site A, disappear at 1273 K in the samples ANY and KAT 1 (Figs. 12.c and 14.c). But, in the BON sample, the intensity of the lines attributed to octahedral $Fe^{3+}$ ions of site B

decreases at 873 K and these lines disappear during the treatment at 1273 K. These results suggest that the thermal dehydroxylation and the structural reorganization make the clay more disordered and disorganizes the octahedral sites by changing the coordination of the $Fe^{3+}$ ions in octahedral position.

**Table 7**
Assignment of resonances observed in the crude ANY, BON and KAT 1 samples.

| Sample | Magnetic field | Assignment |
|---|---|---|
| ANY | wide resonance between 2500 and 4000 G | haematite or goethite or iron gels |
| | 3510 G (g=2.05) | crystal imperfections (holes) |
| BON | 1590 G (g=4.53) | $Fe^{3+}$ ions in octahedral position (site A) |
| | 780 G (g=9.24)<br>1400 G (g=5.15)<br>1850 (g=3.9) | $Fe^{3+}$ ions in octahedral position (site B) |
| | wide resonance between 2000 and 4000 G | haematite or goethite or iron gels |
| KAT 1 | 1590 G (g=4.53) | $Fe^{3+}$ ions in octahedral position (site A) |
| | wide resonance between 2000 and 4000 G | haematite or goethite or iron gels |

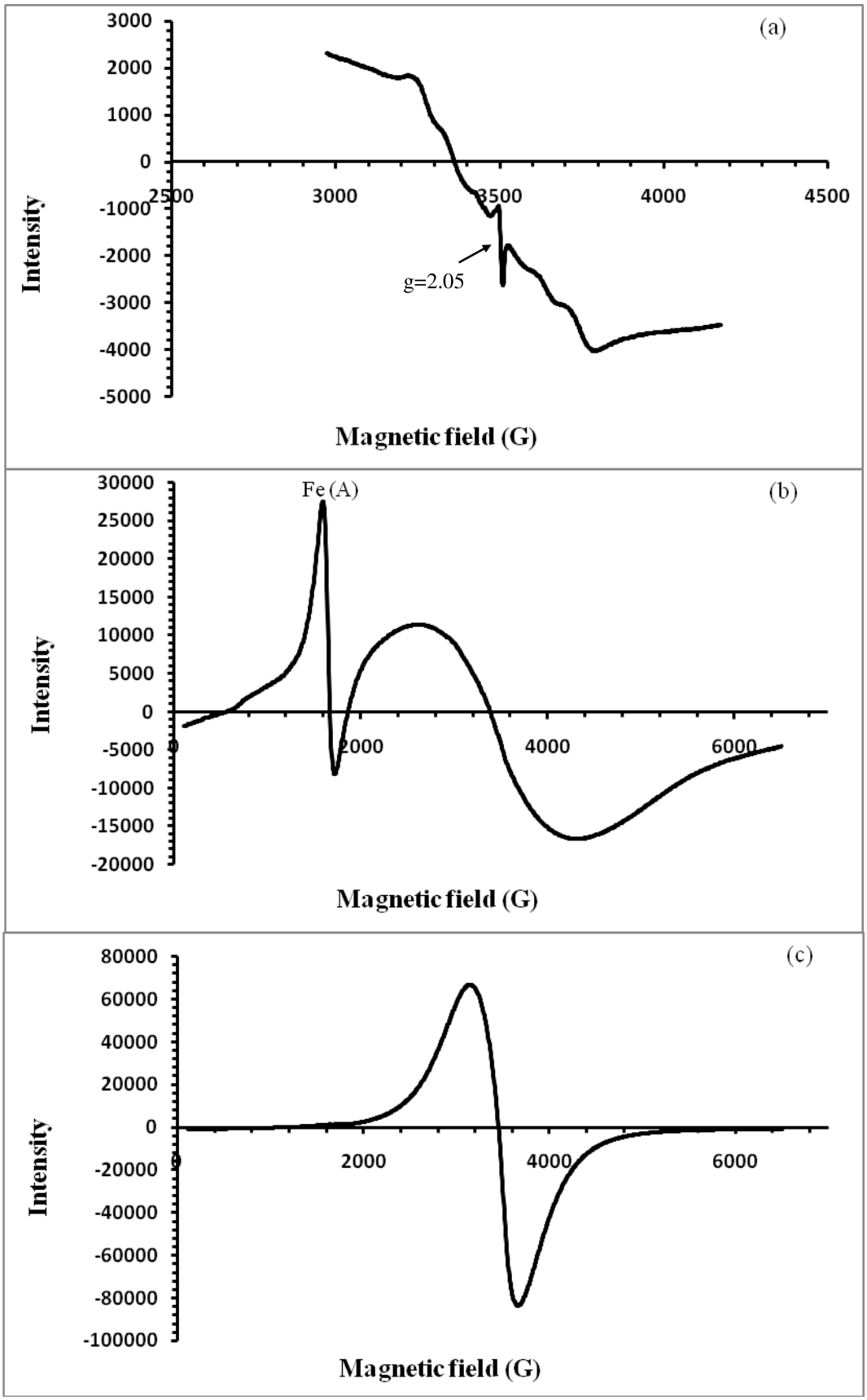


**Fig. 12.** EPR spectra of the ANY sample: (a) raw sample; (b) sample treated at 873 K; (c) sample treated at 1273 K.

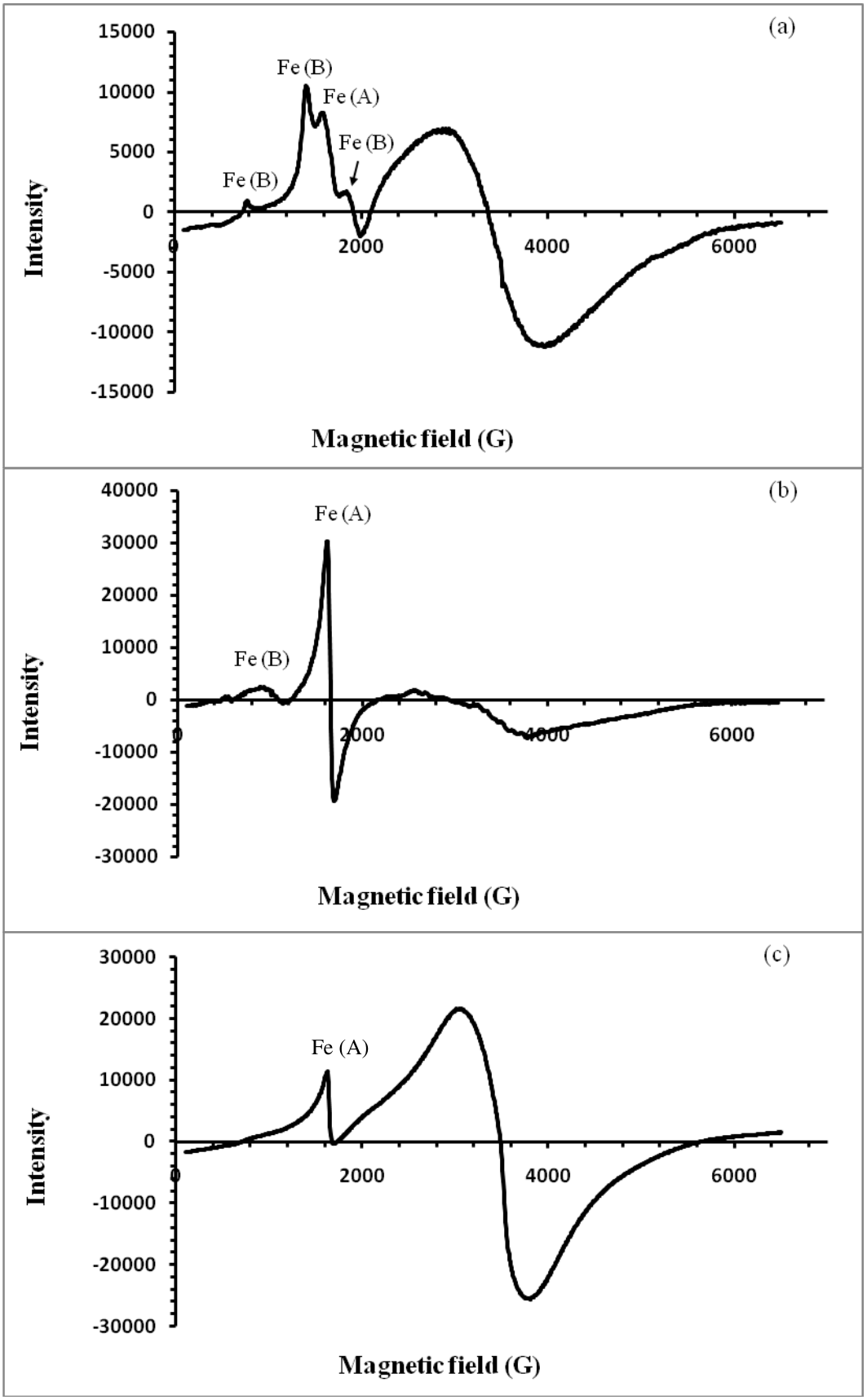


**Fig. 13.** EPR spectra of the BON sample: (a) raw sample; (b) sample treated at 873 K ; (c) sample treated at 1273 K.

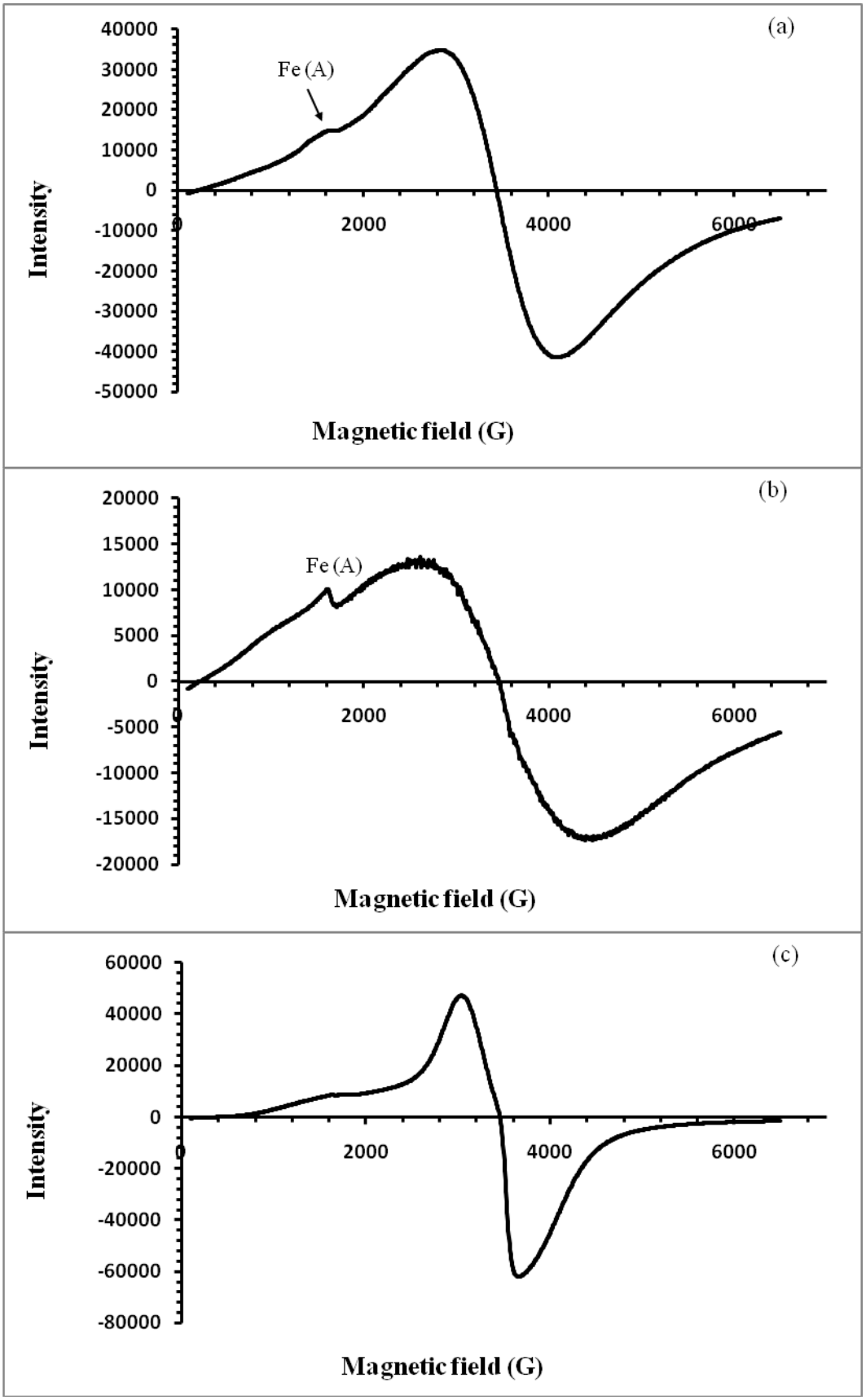


**Fig. 14.** EPR spectra of the KAT 1 sample: (a) raw sample; (b) sample treated at 873 K (c) sample treated at 1273 K.

### 3.10. $^{57}$Fe Mössbauer spectra

The figure 15 shows the $^{57}$Fe Mössbauer spectra of the ANY, BON and KAT 1 samples. The $^{57}$Fe Mössbauer data are shown in table 8. The three samples show quite different Mössbauer spectra but they have in common a paramagnetic iron site noted $Fe^{3+}$ (a), located in a octahedral site distorted. A paramagnetic $Fe^{2+}$ ions site is also present in these three samples. It is located in an octahedral site distorted. The amount of divalent iron ions ($Fe^{2+}$) in samples BON and KAT 1 is low. The KAT 1 sample shows a second octahedral site of $Fe^{3+}$ ions denoted $Fe^{3+}$ (b), having a great quadrupole splitting Δ=2 mm/s. Finally, the ANY sample shows (orange curve) an iron site magnetically ordered which representing 24% of the total spectra. This is an iron oxide ($Fe_2O_3$) in agreement with the sextuplet observed on the spectra realized at +/- 10 mm s$^{-1}$.

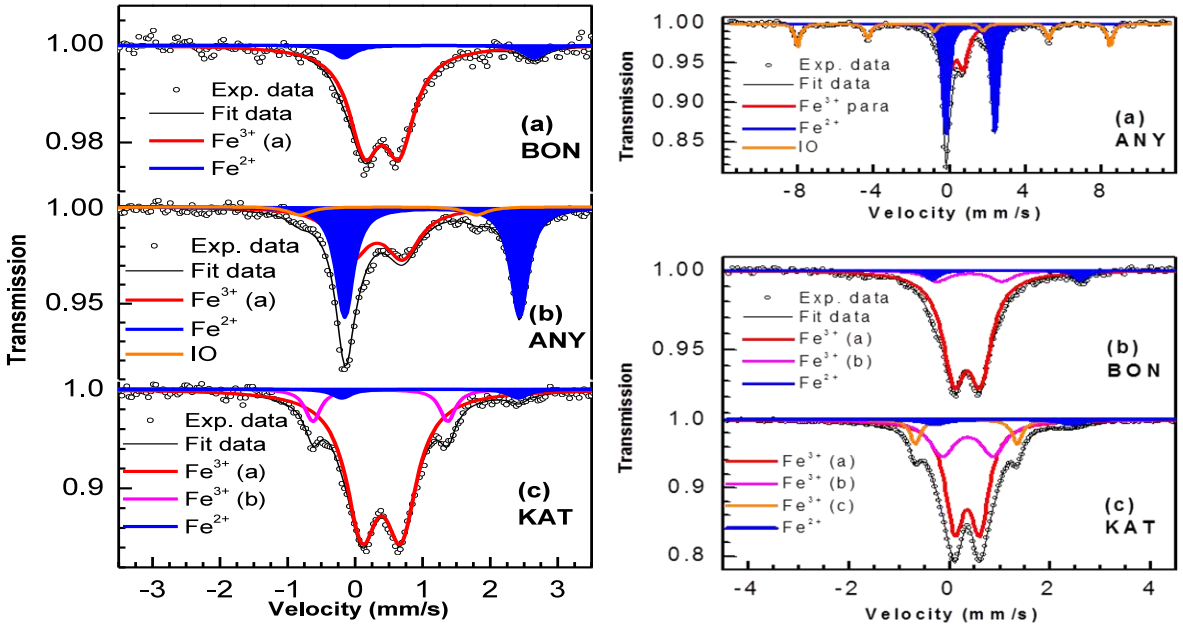


**Fig. 15**. $^{57}$Fe Mössbauer spectra of the ANY, BON and KAT 1 samples.

**Table 8**
$^{57}$Fe Mössbauer datas of BON, ANY and KAT 1 samples.

| Sample | δ (mm/s) | Δ (mm/s) | LW (mm/s) | % | Assignment |
|---|---|---|---|---|---|
| BON | 0.40 ± 0.01 | 0.52 ± 0.02 | 0.55 ± 0.04 | 91 ± 4 | $Fe^{3+}$ (a) |
| | 1.24 ±0.07 | 2.82 ± 0.14 | 0.39 ± 0.21 | 9 ± 4 | $Fe^{2+}$ |
| ANY | 0.32 ± 0.02 | 0.76 ± 0.03 | 0.60 ± 0.04 | 35 ± 8 | $Fe^{3+}$ (a) |
| | 1.14 ± 0.00 | 2.59 ± 0.01 | 0.31 ± 0.01 | 41 ± 3 | $Fe^{2+}$ |
| | 0.59 ± 0.05 | 0.20 ± 0.01 | 0.41 ± 0.12 | 24 ± 5 | ~ $Fe_2O_3$ |
| KAT 1 | 0.39 ± 0.01 | 0.58 ± 0.01 | 0.57 ± 0.02 | 86 ± 3 | $Fe^{3+}$ (a) |
| | 0.37 ± 0.01 | 2.00 ± 0.03 | 0.28 ± 0.05 | 11 ± 2 | $Fe^{3+}$ (b) |
| | 1.11 ± 0.06 | 2.62 ± 0.11 | 0.34 ± 0.17 | 4 ± 1 | $Fe^{2+}$ |

## 4. Conclusion

This work presents the mineralogical, textural and physicochemical characteristics of five clay samples, collected in various regions of Côte d'Ivoire. The characterization techniques used were X-ray diffraction (XRD), scanning electron microscopy (SEM), X-ray fluorescence, Infrared (IR) spectroscopy, Differential Scanning Calorimetry coupled with thermogravimetric analysis, Electron Paramagnetic Resonance (EPR) spectroscopy and Mössbauer $^{57}Fe$ spectroscopy. The measurement of the specific surface and the granulometric analysis were also made.

The characterization by X-ray Diffraction (XRD) and chemical analysis, revealed that samples have a different mineralogical composition with a high proportion of aluminium silicates. Chlorite, kaolinite, smectites, illite, quartz, goethite and rutile are the mineral phases identified. The Scanning Electron Microscopy (SEM) showed hexagonal tablets with regular surface in the BON sample. Infrared spectroscopy led to the chemical functions present in the samples and made it possible the study of their crystallinity. The samples have low crystallinity. They are quite rich in fine particles, their specific surfaces area are relatively important and contain structural iron, iron oxides and oxyhydroxides. The study of the iron occupy environment showed that this metal exists essentially in the trivalent status in octahedral environments. These characteristics could lead to the use of these clay samples in the treatment and depollution of wastewater as adsorbents.

## References

[1] O. Bouras, Adsorptive properties of organophilic bridged clays: Synthesis and Characterization, Thesis, University of Limoges, France (2003).

[2] V. Coulibaly, Contribution to the study of clays consumed in Ivory Coast: Mineralogy, Reactivity under digestive conditions, Radioactivities, Thesis, Université Félix Houphouët Boigny (UFHB), Abidjan, Côte d'Ivoire (2013).

[3] E. Errais (2011), Surface reactivity of natural clays. Study of the adsorption of anionic dyes, Thesis, University of Strasbourg, France (2011).

[4] K.L. Konan (2006), Interactions between clay materials and a basic medium rich in calcium, Thesis, University of Limoges, France (2006).

[5] J. Sei (1998), Study of materials of reduced dimensionality. Structure-property relationship in natural kaolinites from Cote d'Ivoire, Thesis, University of Montpellier II, France (1998).

[6] H. Fabien, Modeling of diffractograms of clay minerals in complex assemblies in two temperate climate soils. Mineralogical and pedological involvement, Thesis, Poitiers University, France (2008).

[7] N.C. Amin, Y.Y.J. Andji, M. Ake, S.F. Yolou, A. Toure-Abba, G. Kra, *Mineralogy and physicochemistry of Buruli ulcer treatment clays in Côte d'Ivoire*, J. Sci. Pharm. Biol. 10(1) (2009) 21-30.

[8] B.I. Battut, The virtues of clay. Equipédia, French Institute of Horse and Horse Riding (2018). http://www.equipedia.ifce.

[9] M.I. Carretero, *Clay minerals and their beneficial effects upon human health: a review*, Applied Clay Science 21 (2002) 155–163.

[10] F. Hernot, Clay, its use at the pharmacy, Thesis in pharmacy, Angers University, France (2016).

[11] L.P.M-S. Kouakou, Y.Y.J. Andji, Y. Coulibaly, *Mineralogy, geochemistry of clay raw material from Ivory Coast (West Africa) used as pharmaceutical products*, J. Soc. Ouest-Afr. Chim. 034 (2012) 38-44.

[12] S.C. Paulo, S.M.B. Oliveira, L. Farias, D.I.T. Fávaro, B.P. Mazzilli, *Chemical and radiological characterization of clay minerals used in pharmaceutics and cosmetics*, Applied Clay Science 52 (2011) 145–149.

[13] C. Viseras, C. Aguzzi, P. Cerezo, A. Lopez-Galindo, *Uses of clay minerals in semisolid health care and therapeutic products*, Applied Clay Science 36 (2007) 37–50.

[14] J. Allègre, Does clay scare Big Pharma? HEALTH/ALTERNATIVES. NEXUS 90 (2014) 34-39.

[15] L.N. Amon, K. L. Konan, D.H. Goure, Y.Y.J. Andji, K.J. Coulibaly, S. Oyetola, *Physico-chemical and structural properties of clay-based ceramic filters from Côte d'Ivoire,* J. Soc. Ouest-Afr. Chem 044 (2017) 70-77.

[16] K.L. Konan, J. Soro, Y.Y.J. Andji, S. Oyetola, G. Kra, *Comparative study of dehydroxylation/amorphination in two kaolins of different crystallinity*, J. Soc. Ouest-Afr. Chimie 030 (2010) 29-39.

[17] A.A. Pierre, K.A. Brice, C. Vamoussa, K. N'Dri, S. Joseph, E.O. Samuel, *Kinetic and Thermodynamic Study of the Dephosphation of Wastewater by Clay Materials from Côte d'Ivoire*, Open Journal of Applied Sciences 11 (2021) 1307-1323.

[18] N. Boualla, A. Benziane, *Experimental study on the removal of nitrates by adsorption on activated and non-activated clays of Olan sebkha (Algeria)*, Africa science 7(2) (2011) 56-73.

[19] R. Saad, Adsorption and Desorption of Phosphate and Nitrate Ions by Silica-Based Mesoporous Materials Functionalized with Ammonium Groups, Thesis, Laval University, Laval, France (2008).

[20] J.Y.Y. Andji, J. Sei, T.A. Abba, G. Kra, D. Njopwouo, *Mineralogical characterization of some clay samples from the GOUNIOUBE site (CÔTE D'IVOIRE)*, J. Soc. Ouest-Afr. Chim. 011 (2001) 143 - 166.

[21] D. Njopwouo, Mineralogy and physicochemistry of the clays of Bomkoul and Balengou (Cameroon). Use in the polymerization of styrene and in the reinforcement of natural rubber, Thesis, University of Yaoundé, Cameroon (1984).

[22] J. Yvon, J. Baudracco, J.M. Cases, J. Weiss, Clay materials, Structure, Properties and Applications: Elements of quantitative mineralogy in microanalysis of clays. A. Decarreau, Ed. French Society of Mineralogy and Crystallography, Paris (1990) 473-489.

[23] J. Sei, A.A. Touré, J. Olivier-Fourcade, H. Quiquampoix, S. Staunton, J.C. Jumas, M. Womes, *Characterisation of Kaolinitic Clays from the Ivory Coast: Identification of Structural Fe*, Hyperfine Interactions 155 (2004) 51-64.

[24] J. Sei, A.A. Touré, S. Oyétola, G. Kra, J.C. Jumas, J. Olivier-Fourcade, *Deferrification of natural kaolinites from Ivory Coast: Study by electron paramagnetic resonance and diffuse reflectance*, J. Soc. Ouest-Afr. Chim. 016 (2003) 59-76.

[25] E. Eslinger, D. Peaver, Clay Minerals for Petroleum Geologists and Engineers, SEPM Short Course Notes No. 22, Society of Economic Paleontologists and Mineralogists, Tulsa (1988).

[26] E. Paterson, R. Swaffield, In a Handbook of Determinative Methods in Clay Mineralogy, Thermal Analysis, Ed. Wilson M. J. (Blackie, Glasgow) (1987) 99-132.

[27] S. Caillère, S. Hénin, M. Rautureau, Mineralogy of clays II, Classification and Nomenclature, 2nd Ed. Masson, Paris (1982).

[28] B. Delvaux, A.J. Herbillon, L. Vielvoye, M.M. Mestdagh, *Surface properties and clay mineralogy of hydrated halloysitic soil clays. II: Evidence for the presence of halloysite/smectite (H/Sm) mixed-layer clays*, Clay Minerals 25(2) (1990) 141-160.

[29] P. Quantin, J. Gautheyrou, P. Lorenzoni, *Halloysite formation through in situ weathering of volcanic glass from trachytic pumices, Vico's volcano, Italy,* Clay Minerals 23(4) (1988) 423-437.

[30] M.W. Carty, *The colloidal nature of kaolinite*, Am. Ceram. Bull. 78 (1999) 72-76.

[31] C. Bich, J. Ambroise, J. Péra, *Influence of degree of dehydroxylation on the pozzolanic activity of metakaolin*, Applied Clay Science 44 (2009) 194-200.

[32] P. Quantin, IR spetroscopy of various forms of allophane, imogolite and halloysite in soils derived from volcanic materials. In : Infrared spectroscopy and quantitative mineralogical analysis of rocks, Study day, ORSTOM-Bondy, France (1993) 39-47.

[33] V.C. Farmer, The infrared spectra of minerals, Mineralogical Society, London (1974) 331-363.

[34] J.D. Russell, V.C. Farmer, B. Velde, *Replacement of OH by OD in layer silicates and identification of the vibrations of these groups in infrared spectra,* Mineralogical Magazine 37 (1970) 869-879.

[35] J.D. Russell, A.R. Fraser, Infrared Methods. In: M.J. Wilson Ed., Clay Mineralogy: Spectroscopic and Chemical Determinative Methods, Chapman & Hall, London (1994) 11-67.

[36] F. Gezahegn, B. Wasse, F. Nestor, *Removal of nitrate ion from aqueous solution by modified ethiopian bentonite clay*, International Journal of Research in Pharmacy and Chemistry (IJRPC) 4(1) (2014) 192-201.

[37] M. Gourouza, A. Zanguina, I. Natatou, A. Boos, Characterization of a mixed clay of Niger, Rev. CAMES-Sciences Struct. Mat. 1 (2013) 29 - 39.

[38] M. Hajjaji, S. Kacim, M. Boulmane, *Mineralogy and firing characteristics of clay from the valley of Ourika (Morocco)*, Applied Clay Science 21 (2001) 203-212.

[39] A. Qlihaa, S. Dhimni, F. Melrhaka, N. Hajjaji, A. Srhiri, *Physicochemical characterization of a Moroccan clay*, J. Mater. Environ. Sci. 7(5) (2016) 1741-1750.

[40] F. Zibouche, N. Boudissa, A. Irekti, M.T. Abadlia, *Geopolymerization of aluminosilicates. Influence of Silica/Alumina ratios*, Journal of Materials, Processes and Environment 1(2) (2013) 147-156.

[41] Y. Chenc, G.S. Lan, H. Tuanw, *Microstructural evolution of mullite during the sintering of kaolin powder compacts*, Ceramics International 26 (2000) 715-720.

[42] N.S. Soro, Influence of iron ions on the thermal transformations of kaolinite, Thesis, University of Limoges, France (2003).

[43] D.B.I.H. Goure, Study of the consolidation of “geomimetic” materials based on lateritic clay: effect of acids and ferric phases, Thesis, University of Limoges, France (2013).

[44] J. Sei, J.C. Jumas, J. Olivier-Fourcade, H. Quiquampoix, S. Staunton, *Role of iron oxides in the phosphate adsorption properties of kaolinites from the ivory coast*, Clays and Clay Minerals 50(2) (2002) 219 - 224.

[45] N. Soro, L. Aldon, J. Olivier-Fourcade, J.C. Jumas, J.P. Laval, P. Blanchart, *Role of Iron in Mullite Formation from Kaolins by Mössbauer Spectroscopy and Rietveld Refinement*, J. Am. Ceram. Soc. 86(1) (2003) 129-134.

[46] D. Bonnin, S. Muller, G. Calas, *The iron in the kaolins. Study by spectrometry RPE, Mössbauer, EXAFS*, Bulletin de Minéralogie 105 (1982) 467-475.

[47] T. Delineau, T. Allard, J.P. Muller, O. Barres, J. Yvon, J.M. Cases, *FTIR Reflectance vs. EPR studies of structural iron in kaolinites*, Clays and Clay Minerals 42 (1994) 308-320.